*Sixth Iberian Robotics Conference (ROBOT 2023), Coimbra, Portugal, November 22-24, 2023*

# Adaptive Control for a Quadrotor with Ceiling Effect Estimate

Pedro Outeiro, Carlos Cardeira, and Paulo Oliveira

IDMEC, Instituto Superior Técnico, Universidade de Lisboa,
Avenida Rovisco Pais, 1049-001 Lisbon, Portugal,
pedro.outeiro@tecnico.ulisboa.pt

**Abstract.** This paper presents an adaptive solution for the control of a quadrotor operating close to the ceiling. The vicinity alters the flow resulting on a variation on the effective thrust. A force factor is estimated in real time using an adaptive mechanism. The full controller is proven to have global asymptotic stability with zero tracking error using Lyapunov theory. The resulting system is validated in simulation with approaching trajectories to the ceiling, and its robustness is shown for mass variations of up to 20%.

**Keywords:** Adaptive Control, Parameter Estimation, Autonomous Aerial Vehicles, Ceiling Effect

## 1 Introduction

Quadrotors have had a growing interest in their application for inspection and maintenance of infrastructures, such as concrete bridges [12]. In these applications, the quadrotor has to be in the proximity of ceiling surfaces that affect the airflow from the rotors and affect the thrust generated. This presents a major control concern, as it provided an unknown in the actuation of the autonomous system. This paper focuses on the ceiling effect, and provides an adaptive control solution for the problem at hand.

Control methods for multirotors can be seen in [18, 15, 11, 13, 2, 9, 17, 3]. A trajectory tracking controller using $\mathscr{L}_1$ adaptive control, for quadrotors with time-varying aerodynamic effect and bounded external disturbance, is proposed in [18]. A model-free-based terminal sliding mode control strategy, for quadrotor with parameter variations, uncertainties, and external disturbances, is presented in [15]. A robust attitude quadrotor control based on a fractional order PI nonlinear structure is proposed and experimentally validated in [11]. A hierarchical control architecture using a multi-input fast nonsingular terminal sliding mode control strategy is presented in [13]. A method based on saturated feedback and backstepping control is proposed in [2], which is robust to persistent disturbances. A state-dependent Riccati equation controller using the artificial potential field method is proposed in [9], for collision avoidance in cooperative hexarotors with manipulators. In [17], a global saturated tracking controller for a quadrotor is proposed, and experimental validation is provided. An output feedback controller for quadrotors using neural networks is delineated in [3].

The ceiling effect on quadrotors has been studied and modeled in [16, 5, 4]. A potential model was developed using momentum theory, blade element theory and a

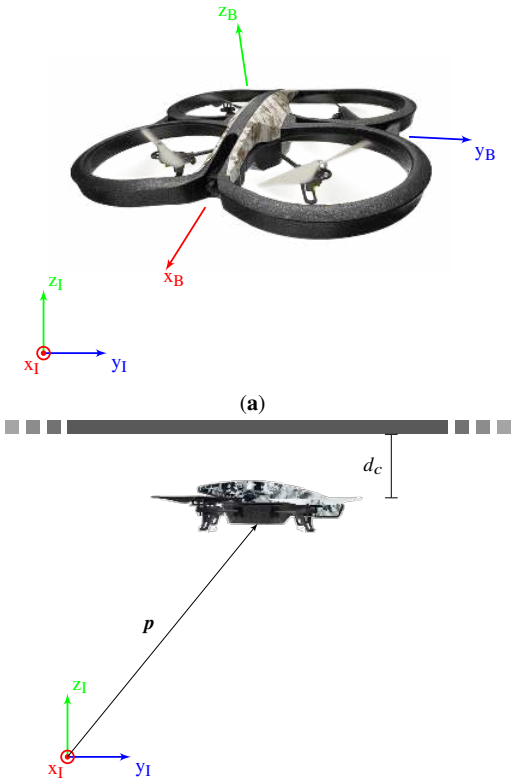


Fig. 1: Quadrotor and Ceiling Setup.

model of ”ground effects”. The resulting model is calibrated using a simulation in ANSYS [16]. Momentum theory and blade element theory are also used in [5] to model the ceiling effect. The model is validated using four propellers in a quadrotor configuration and a force sensor. In [4], the lift and flow field are analyzed to model the ceiling effect for a Crazyflie quadrotor. Additionally, this model is used to provide more energy efficient trajectories for a quarotor traveling near surfaces.

Control approaches that account for the ceiling effect are presented in [7, 1, 10]. MPC control is considered in both [7] and [1], while [10] proposes an in-unsteady-state-model-based controller.

This work addresses the problem of controlling a quadrotor operating near the ceiling. The presented solution is an adaptive controller, and is tested in simulation. The force factor is directly estimated by an adaptive mechanism, and is used to adjust the control.

The main contribution of this paper is the proposal of an adaptive mechanism where the force factor is directly estimated and is used to adjust the control. Moreover,

the system is proven to have global asymptotic stability with zero tracking error and uncertainty in the force factor using Lyapunov theory.

The notation used for scalars, vectors, and matrices is lowercase, bold lowercase, and bold uppercase, respectively. Additionally, $\|\cdot\|$ represents the norm of a vector.

This paper is organized as follows: the problem is presented in Section 2. The proposed controller is explained in Section 3. The stability of the controller is proven in Section 4. Simulation results are presented and discussed in Section 5. Finally, some concluding remarks are drawn in Section 6.

## 2 Problem Statement

Following a by now classical approach described in [8], consider an inertial reference frame $\{\mathrm{I}\}$ of the quadrotor with upward z and forward x, as depicted in Fig. 1. The position of the quadrotor is denoted as $\boldsymbol{p} \in \mathbb{R}^3$. The rotation matrix from the body fixed frame $\{\mathrm{B}\}$, relative to $\{\mathrm{I}\}$, is given by $\boldsymbol{R} \in \mathbb{R}^{3\times3}$. The body-frame angular velocity is denoted by $\boldsymbol{\omega} \in \mathbb{R}^3$. The thrust and torque are denoted by $f \in \mathbb{R}$ and $\boldsymbol{\tau} \in \mathbb{R}^3$, respectively. The mass of the system is $m \in \mathbb{R}$. The inertia of the drone is $\boldsymbol{J} \in \mathbb{R}^{3\times3}$, and is positive definite. The gravity constant is $g \in \mathbb{R}$. $\boldsymbol{e}_3$ is the vector $[0 \;\; 0 \;\; 1]^T$. The dynamics of a quadrotor are, therefore,

$$m\ddot{\boldsymbol{p}} = (f\boldsymbol{R} - mg)\,\boldsymbol{e}_3, \tag{1}$$

$$\dot{\boldsymbol{R}} = \boldsymbol{R}\boldsymbol{\omega}_\times, \tag{2}$$

$$\boldsymbol{J}\dot{\boldsymbol{\omega}} = -\boldsymbol{\omega} \times \boldsymbol{J}\boldsymbol{\omega} + \boldsymbol{\tau}. \tag{3}$$

To account for the ceiling effect, a force factor $a$ is added to (1):

$$m\ddot{\boldsymbol{p}} = (af\boldsymbol{R} - mg)\,\boldsymbol{e}_3. \tag{4}$$

The behavior of the ceiling effect (and ground effect) was studied in [4]. This paper suggested the use of an inverse power law to describe the relation between the lift ($l \in \mathbb{R}$) produced in the proximity of a surface and at infinite distance ($l_\infty \in \mathbb{R}$) from any surface:

$$a = \frac{l}{l_\infty} = \frac{\beta_1}{d^*} + \beta_2. \tag{5}$$

This model uses two model parameters $\beta_1$ and $\beta_2$, and a nondimentionalized distance $d^*$ that depends on the rotor radius $r$ defined as

$$d^* = \frac{d}{r}. \tag{6}$$

The use of the nondimentionalized distance generalizes the model for different quadrotors, and is shared with other models.

For model completeness, both the ground and ceiling effects are considered, and the overall model in this paper is obtained using the maximum of each effect and 1. The resulting formulation is

$$a = \max\left(\frac{\beta_{1c}}{d_c^*} + \beta_{2c},\; \frac{\beta_{1g}}{d_g^*} + \beta_{2g},\; 1\right), \tag{7}$$

where $\beta_{1c}$, $\beta_{2c}$, $\beta_{1g}$, and $\beta_{2g}$ are model parameters, $d_c^*$ is the nondimentionalized distance to the ceiling, and $d_g^*$ is the nondimentionalized distance to the ground.

The objective of this paper is to design an adaptive stable controller for the presented formulation, capable of handling uncertainty in the ceiling effect by estimating the value of the variable $a$.

## 3 Control

The controller presented in this paper is based on [14]. The first step in designing the controller is determining the desired force $\boldsymbol{f}_d \in \mathbb{R}^3$. At this stage, the orientation of the quadrotor is not relevant, therefore it can be formulated as

$$\boldsymbol{f}_d = -k_1 \boldsymbol{e}_p - k_2 \dot{\boldsymbol{e}}_p + \hat{b} m \left( \ddot{\boldsymbol{p}}_d + g \boldsymbol{e}_3 \right), \tag{8}$$

where $\boldsymbol{e}_p = \boldsymbol{p} - \boldsymbol{p}_d$ is the position error, $\boldsymbol{p}_d$ is the desired position, $k_1 \in \mathbb{R}$ is the position control gain, $k_2 \in \mathbb{R}$ is the velocity control gain, and $\hat{b}$ is the estimate of the parameter $b = a^{-1}$. Additionally, the desired force provides a desired heading

$$\boldsymbol{h}_d = \frac{\boldsymbol{f}_d}{\left\| \boldsymbol{f}_d \right\|}. \tag{9}$$

To adjust the rotation of the system, a desired angular velocity $\boldsymbol{\omega}_d$ is designed as

$$\boldsymbol{\omega}_d = S(\boldsymbol{e}_3) R^T \left[ \boldsymbol{C}^T \dot{\boldsymbol{h}}_d + k_3 \boldsymbol{h}_d - k_4 \left\| \boldsymbol{f}_d \right\| \left( \epsilon \boldsymbol{e}_p + \dot{\boldsymbol{e}}_p \right) \right], \tag{10}$$

$$\boldsymbol{C} = \left( \boldsymbol{h}_d \cdot \boldsymbol{R} \boldsymbol{e}_3 \right) \boldsymbol{I}_3 + S(\boldsymbol{R} \boldsymbol{e}_3 \times \boldsymbol{h}_d), \tag{11}$$

where $k_3 \in \mathbb{R}$ and $k_4 \in \mathbb{R}$ are control gains, $\epsilon \in \mathbb{R}$ is a tuning parameter, and $S(\boldsymbol{a})$ is the skew-symmetric matrix of a vector $\boldsymbol{a} \in \mathbb{R}^3$ ($\boldsymbol{a}, \boldsymbol{b} \in \mathbb{R}^3, \boldsymbol{a} \times \boldsymbol{b} = S(\boldsymbol{a}) \boldsymbol{b}$).

Using $\boldsymbol{f}_d$ and $\boldsymbol{\omega}_d$, the actuation provided by the controller is designed as

$$f = \boldsymbol{f}_d \cdot \boldsymbol{R} \boldsymbol{e}_3 = \boldsymbol{R}^T \boldsymbol{f}_d \cdot \boldsymbol{e}_3, \tag{12}$$

$$\boldsymbol{\tau} = \boldsymbol{\omega} \times \boldsymbol{J} \boldsymbol{\omega} + \boldsymbol{J} \dot{\boldsymbol{e}}_\omega - k_5 \boldsymbol{e}_\omega + k_6 S\left( \boldsymbol{e}_3 \right) \boldsymbol{R}^T \boldsymbol{h}_d, \tag{13}$$

with $\boldsymbol{e}_\omega = \boldsymbol{\omega} - \boldsymbol{\omega}_d$ and $k_5 \in \mathbb{R}$ being the angular velocity error and control gain, respectively. Additionally, $k_6 \in \mathbb{R}$ is also a control gain.

The final component of the control is the adaptive mechanism used to estimate $b$. It is formulated as

$$\dot{\hat{b}} = -\frac{k_7}{m} \left( g \boldsymbol{e}_3 + \ddot{\boldsymbol{p}}_d \right)^T \left( \epsilon \boldsymbol{e}_p + \dot{\boldsymbol{e}}_p \right). \tag{14}$$

The behavior of the estimate is adjusted using the $k_7 \in \mathbb{R}$ gain and the tuning parameter $\epsilon$.

## 4 Controller Stability

The stability of the proposed control solution is proven to have global asymptotic tracking stability using a Lyapunov function $V$. The first part of the Lyapunov candidate function

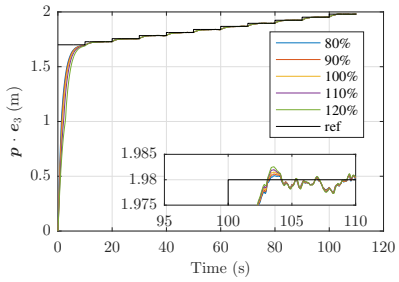


(**a**) $z$ Position

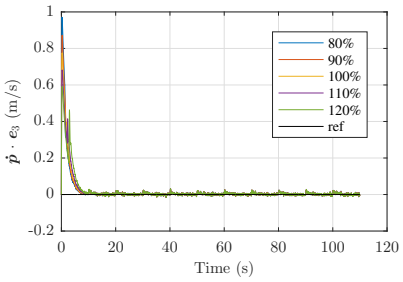


(**b**) $z$ Velocity

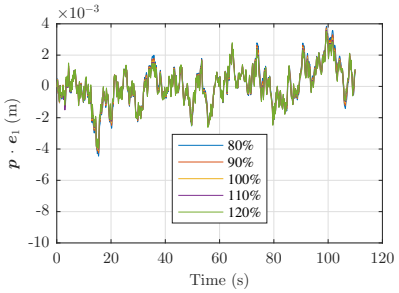


(**c**) $x$ Position

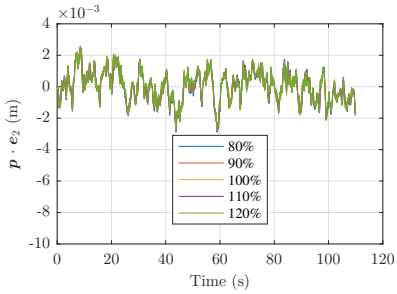


(**d**) $y$ Position

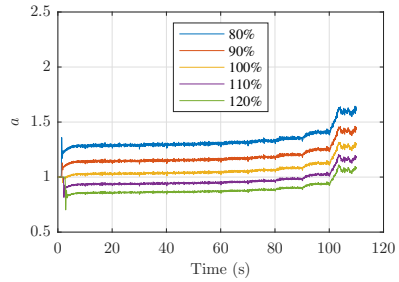


(**e**) $a$ Estimate in Time

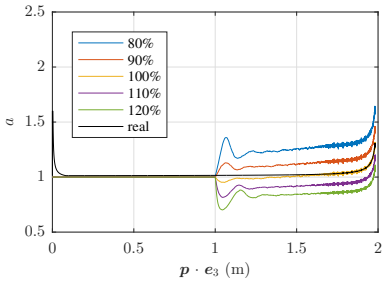


(**f**) $a$ Estimate in Height

Fig. 2: Simulation Results for Step Trajectory.

$W_1$, used to construct the function, is formulated as

$$W_1 = \frac{1}{2}\boldsymbol{e}_\eta^T \boldsymbol{P} \boldsymbol{e}_\eta, \quad \boldsymbol{\eta} = \begin{bmatrix} \dot{\boldsymbol{p}} \\ \boldsymbol{p} \end{bmatrix}, \quad \boldsymbol{e}_\eta = \begin{bmatrix} \dot{\boldsymbol{e}}_p \\ \boldsymbol{e}_p \end{bmatrix}$$
$$\boldsymbol{P} = \begin{bmatrix} bm\boldsymbol{I}_3 & \epsilon bm\boldsymbol{I}_3 \\ \epsilon bm\boldsymbol{I}_3 & (k_1 + \epsilon k_2)\,\boldsymbol{I}_3 \end{bmatrix}. \tag{15}$$

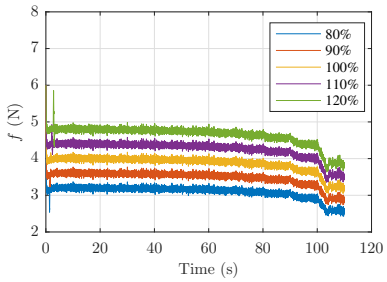


(**a**) Thrust in Time

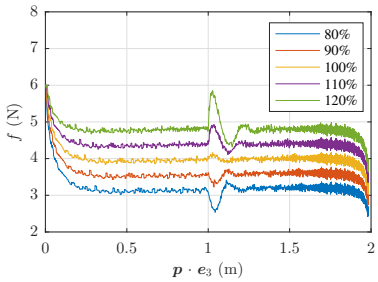


(**b**) Thrust in Height

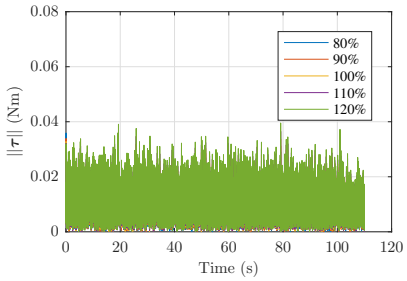


(**c**) Torque Norm

Fig. 3: Simulation Results for Step Trajectory Continued

To determine its derivative, the required acceleration error $\ddot{\boldsymbol{e}}_p$ is formulated using $e_b = \hat{b} - b$, yielding

$$
\begin{aligned}
m\ddot{\boldsymbol{e}}_p &= -m\left(g\boldsymbol{e}_3 + \ddot{\boldsymbol{p}}_d\right) + af\boldsymbol{R}\boldsymbol{e}_3 \\
\Leftrightarrow bm\ddot{\boldsymbol{e}}_p &= -bm\left(g\boldsymbol{e}_3 + \ddot{\boldsymbol{p}}_d\right) + \left(\boldsymbol{R}^T\boldsymbol{f}_d \cdot \boldsymbol{e}_3\right)\boldsymbol{R}\boldsymbol{e}_3 \\
&= e_b m\left(g\boldsymbol{e}_3 + \ddot{\boldsymbol{p}}_d\right) + \boldsymbol{R}\boldsymbol{e}_3\left(\boldsymbol{R}^T\boldsymbol{f}_d \cdot \boldsymbol{e}_3\right) - k_1\boldsymbol{e}_p \\
&\quad - k_2\dot{\boldsymbol{e}}_p - \boldsymbol{f}_d \\
&= e_b m\left(g\boldsymbol{e}_3 + \ddot{\boldsymbol{p}}_d\right) + \boldsymbol{R}\left(\boldsymbol{e}_3\boldsymbol{e}_3^T - \boldsymbol{I}_3\right)\boldsymbol{R}^T\boldsymbol{f}_d \\
&\quad - k_1\boldsymbol{e}_p - k_2\dot{\boldsymbol{e}}_p \\
&= e_b m\left(g\boldsymbol{e}_3 + \ddot{\boldsymbol{p}}_d\right) - \boldsymbol{R}\boldsymbol{\Gamma}\boldsymbol{R}^T\boldsymbol{f}_d - k_1\boldsymbol{e}_p - k_2\dot{\boldsymbol{e}}_p.
\end{aligned}
\tag{16}
$$

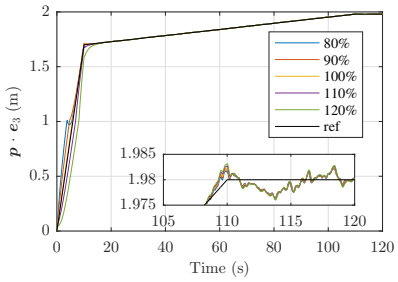


(**a**) $z$ Position

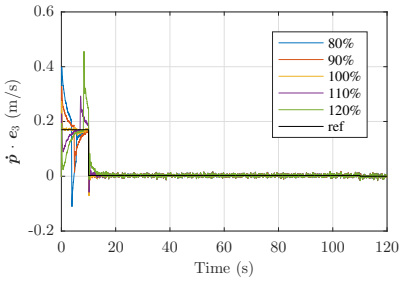


(**b**) $z$ Velocity

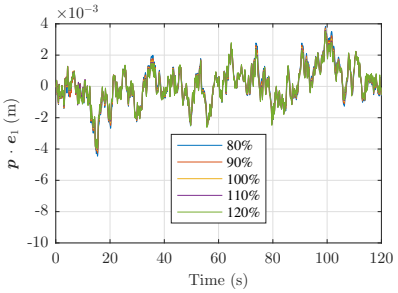


(**c**) $x$ Position

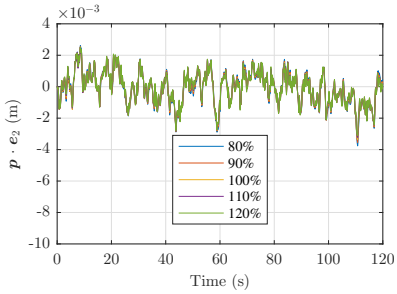


(**d**) $y$ Position

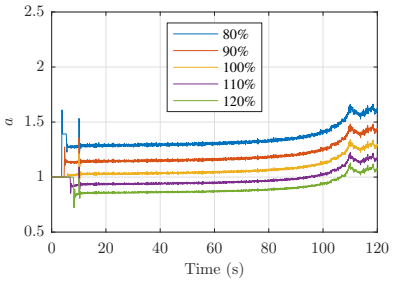


(**e**) $a$ Estimate in Time

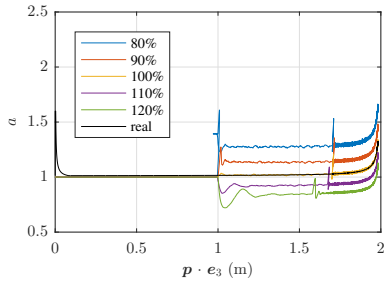


(**f**) $a$ Estimate in Height

Fig. 4: Simulation Results for Ramp Trajectory.

The resulting $\dot{W}_1$ is, therefore,

$$\begin{aligned}\dot{W}_1 = &- \boldsymbol{e}_\eta^T \boldsymbol{Q} \boldsymbol{e}_\eta + e_b m \left(g\boldsymbol{e}_3 + \ddot{\boldsymbol{p}}_d\right)^T \left(\epsilon \boldsymbol{e}_p + \dot{\boldsymbol{e}}_p\right) \\ &- \|f_d\| \boldsymbol{R}^T \left(\epsilon \boldsymbol{e}_p + \dot{\boldsymbol{e}}_p\right) \cdot \boldsymbol{\Gamma} \boldsymbol{R}^T \boldsymbol{h}_d \\ \boldsymbol{Q} = &\begin{bmatrix} (k_2 - \epsilon b m)\, \boldsymbol{I}_3 & 0 \\ 0 & \epsilon k_1 \boldsymbol{I}_3 \end{bmatrix}.\end{aligned} \tag{17}$$

So long as $(k_2 - \epsilon bm) > 0$, $\boldsymbol{Q}$ is positive definite.

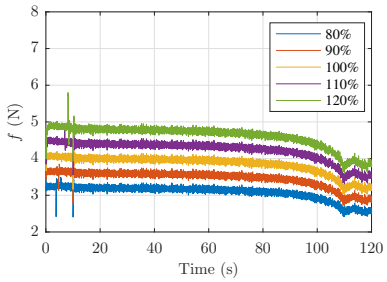


(**a**) Thrust in Time

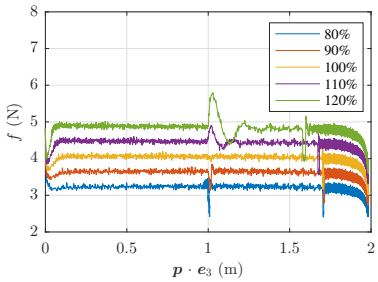


(**b**) Thrust in Height

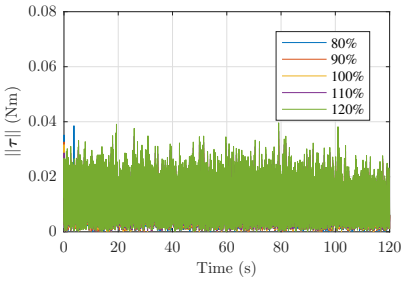


(**c**) Torque Norm

Fig. 5: Simulation Results for Ramp Trajectory Continued.

The second part of the Lyapunov candidate is $W_2 = 1 - \boldsymbol{h}_d \cdot \boldsymbol{R}\boldsymbol{e}_3$. Using the properties $\boldsymbol{h}_d \cdot \dot{\boldsymbol{h}}_d = 0$ (since $\|\boldsymbol{h}_d\| = 1$), and $\boldsymbol{R}^T\boldsymbol{h}_d \cdot \boldsymbol{\Gamma}\boldsymbol{R}^T\boldsymbol{h}_d = 1 - \left(\boldsymbol{R}^T\boldsymbol{h}_d \cdot \boldsymbol{e}_3\right)^2$ (since $\left\|\boldsymbol{R}^T\boldsymbol{h}_d\right\| = 1$) provides

$$\begin{aligned}\dot{W}_2 = &- k_3\left(1 - \left(\boldsymbol{R}^T\boldsymbol{h}_d \cdot \boldsymbol{e}_3\right)^2\right) - \boldsymbol{h}_d \cdot \boldsymbol{R}S\left(\boldsymbol{e}_\omega\right)\boldsymbol{e}_3 \\ &+ k_4\left\|\boldsymbol{f}_d\right\|\boldsymbol{R}^T\left(\epsilon\boldsymbol{e}_p + \dot{\boldsymbol{e}}_p\right) \cdot \boldsymbol{\Gamma}\boldsymbol{R}^T\boldsymbol{h}_d.\end{aligned} \tag{18}$$

The third part of the Lyapunov candidate is

$$W_3 = \frac{1}{2}\boldsymbol{e}_\omega^T\boldsymbol{J}\boldsymbol{e}_\omega. \tag{19}$$

To determine its derivative, the required angular acceleration error $\dot{\boldsymbol{e}}_\omega$ is formulated using (3) and (13), which yields

$$\boldsymbol{J}\dot{\boldsymbol{e}}_\omega = -k_5\boldsymbol{e}_\omega + k_6 S\left(\boldsymbol{e}_3\right)\boldsymbol{R}^T\boldsymbol{h}_d. \tag{20}$$

Therefore, the derivative of the third part of the Lyapunov candidate is

$$\dot{W}_3 = -k_5\boldsymbol{e}_\omega^2 + k_6\boldsymbol{h}_d \cdot \boldsymbol{R}S\left(\boldsymbol{e}_\omega\right)\boldsymbol{e}_3. \tag{21}$$

Combining the three parts of the Lyapunov candidate, provides

$$W = W_1 + \frac{W_2}{k_4} + \frac{W_3}{k_4 k_6}, \tag{22}$$

that is a positive definite function. However, its derivative

$$\begin{aligned} \dot{W} = &- \boldsymbol{e}_\eta^T \boldsymbol{Q} \boldsymbol{e}_\eta - \frac{k_3}{k_4}\left(1 - \left(\boldsymbol{R}^T \boldsymbol{h}_d \cdot \boldsymbol{e}_3\right)^2\right) \\ &- \frac{k_5}{k_4 k_6} \boldsymbol{e}_\omega^2 + \left(g\boldsymbol{e}_3 + \ddot{\boldsymbol{p}}_d\right) \cdot \left(\epsilon \boldsymbol{e}_p + \dot{\boldsymbol{e}}_p\right), \end{aligned} \tag{23}$$

is not negative definite. To remove the concerning parts of $\dot{W}$, the function

$$V = W + \frac{m^2}{2k_7} e_b^2 > 0 \tag{24}$$

is defined, which has a derivative

$$\dot{V} = -\boldsymbol{e}_\eta^T \boldsymbol{Q} \boldsymbol{e}_\eta - \frac{k_3}{k_4}\left(1 - \left(\boldsymbol{R}^T \boldsymbol{h}_d \cdot \boldsymbol{e}_3\right)^2\right) - \frac{k_5}{k_4 k_6} \boldsymbol{e}_\omega^2. \tag{25}$$

So long as $\boldsymbol{Q}$ is positive definite for any value of $b$, $\dot{V} \leq 0$ assuring that the system has tracking stability. This is achieved by selecting a large enough $k_2$, see (17). To prove that the system has globally asymptotic stability, Barbalat's Lemma [6] is used. Therefore, it is necessary to analyze $\ddot{V}$.

Since it was proven that $\dot{V} \leq 0$, it follows that $\boldsymbol{e}_p$, $\dot{\boldsymbol{e}}_p$, $\boldsymbol{e}_\omega$, and $e_b$ are bounded. The derivative of (25) yields

$$\begin{aligned} \ddot{V} = &\, 2k_1\left(\frac{k_2}{bm} - 2\epsilon\right) \boldsymbol{e}_p^T \dot{\boldsymbol{e}}_p + 2k_2\left(\frac{k_2}{bm} - \epsilon\right) \dot{\boldsymbol{e}}_p^2 \\ &+ 2\left(\frac{k_2}{b} - \epsilon m\right) \dot{\boldsymbol{e}}_p^T \left[\frac{1}{m} \boldsymbol{R} \boldsymbol{\Gamma} \boldsymbol{R}^T \boldsymbol{f}_d - e_b \left(g\boldsymbol{e}_3 + \ddot{\boldsymbol{p}}_d\right)\right] \\ &+ \frac{2k_3}{k_4} \boldsymbol{R}^T \boldsymbol{h}_d \cdot \boldsymbol{e}_3 \left(\boldsymbol{R}^T \dot{\boldsymbol{h}}_d \cdot \boldsymbol{e}_3 + \boldsymbol{R}^T \boldsymbol{h}_d \cdot S(\boldsymbol{\omega}) \boldsymbol{e}_3\right) \\ &+ \frac{2k_5}{k_4} \boldsymbol{e}_\omega^T \boldsymbol{J}^{-1} \left(\frac{k_5}{k_6} \boldsymbol{e}_\omega - S(\boldsymbol{e}_3) \boldsymbol{R}^T \boldsymbol{h}_d\right), \end{aligned} \tag{26}$$

where $\boldsymbol{f}_d$, $\boldsymbol{h}_d$, and $\dot{\boldsymbol{h}}_d$ are bounded. $\ddot{\boldsymbol{p}}_d$ is provided by the proposed trajectory, which ensures it is bounded. Therefore, $\ddot{V}$ is bounded and $\dot{V}$ is uniformly continuous in $t \in [0, \infty)$ and negative definite. From Barbalat's Lemma, it follows that the zero equilibrium of tracking errors is globally asymptotically stable.

## 5 Simulation Results

The proposed solution is tested in simulation with trajectories that gradually approach the ceiling. The first trajectory uses steps for the approach, and the second uses a ramp.

The ceiling is 2 meters high. The adaptive estimation is only activated after a 1 meter height is reached. The model parameters are presented in Table 1. The control gains, obtained through tuning, used are presented in Table 2. Furthermore, for robustness study purposes, the tests are performed with mass variations of up to 20% from the model mass used for the design of the controller.

Table 1: Model Parameters.

| Parameter | Value |
|---|---|
| $m$ (kg) | 0.42 |
| $J_x$ (kg m$^2$) | $2.2383 \times 10^{-3}$ |
| $J_y$ (kg m$^2$) | $2.9858 \times 10^{-3}$ |
| $J_z$ (kg m$^2$) | $4.8334 \times 10^{-3}$ |

Table 2: Control Gains.

| Gain | Value | Gain | Value |
|---|---|---|---|
| $k_1$ | 2 | $k_5$ | $10^{-4}$ |
| $k_2$ | 4 | $k_6$ | 0.8 |
| $k_3$ | $1.25 \times 10^{-1}$ | $k_7$ | $5 \times 10^{-2}$ |
| $k_4$ | 3 | $\epsilon$ | 0.6 |

The results of the first set of simulations are presented in Figs. 2 and 3. The settling times (95%) are of 5 seconds and there is no overshoot. Furthermore, the ceiling height is never reached, despite the presence of sensor noise in the simulations. The estimate of the force factor converges in under 1 second in the following steps. The estimate for the baseline case (100%) follows the real value in terms of height. As expected, the estimate and the thrust vary between the different cases. However, the performance does not degrade with deviations from the model mass. The thrust evolves as desired, decreasing as the quadrotor approaches the ceiling. Finally, the controller was also capable of maintain the $x$ and $y$ positions in the vicinity of the origin with millimetric deviation using adequate torque.

The results of the second set of simulations are presented in Figs. 4 and 5(**c**). The control is capable of tracking the trajectory in the baseline case, despite the estimation activating after the lift-off. For the other cases, the tracking performance is poor before the estimation begins and improves drastically after its activation. The worst performance is observed in the 120% case, only catching up to the trajectory after 14 seconds. The ceiling height is never reached, despite the presence of sensor noise in the simulations. The estimate of the force factor for the baseline case converges in under 1 second, and accompanies closely the real value in terms of height. As expected, the estimate and the thrust vary between the different cases. However, the performance only decreased while catching up to the trajectory after the estimation began. The added noise after 1.7 meters is due to the slower velocity of the second ramp, which results in more frequent smaller adjustments of the position. The thrust evolves as desired, decreasing as the quadrotor

approaches the ceiling. Finally, the controller was also capable of maintain the $x$ and $y$ positions in the vicinity of the origin with millimetric deviation using adequate torque.

## 6 Conclusion

This paper presented an adaptive solution for the control of a quadrotor considering ceiling effect. The full controller is proven to have global asymptotic tracking stability using a Lyapunov theory. Simulations results with mass variations of up to 20% were presented with fast settling times and good tracking. Furthermore, tests performed under nominal conditions yielded accurate estimates of the ceiling effect. With mass variations, the estimates were inaccurate (as expected), but only caused a minor performance drop when testing using a ramp trajectory. Furthermore, the controller was capable of holding the $x$ and $y$ positions with minimal deviation.

## Acknowledgements

This work was financed by national funds through FCT—Foundation for Science and Technology, I.P., through IDMEC, under LAETA, Projects UIDB/ 50022/2020, CAPTURE (PTDC/EEIAUT/ 1732/2020), and by the European Union under the Next Generation EU, through a grant of the Portuguese Republic's Recovery and Resilience Plan (PRR) Partnership Agreement, within the scope of the project PRODUTECH R3 – "Agenda Mobilizadora da Fileira das Tecnologias de Produção para a Reindustrialização", aiming the mobilization of the production technologies industry towards of the reindustrialization of the manufacturing industrial fabric (Project ref. nr. 60 - C645808870-00000067). This work was also supported by FCT through the scholarship SFRH/BD/ 147035/2019.

## References

1. B. B. Kocer, T. Tjahjowidodo, and G. G. L. Seet: Centralized predictive ceiling interaction control of quadrotor vtol uav. Aerospace Science and Technology **76**, 455–465 (2018). DOI https://doi.org/10.1016/j.ast.2018.02.020. URL `https://www.sciencedirect.com/science/article/pii/S1270963817315572`
2. Casau, P., Sanfelice, R.G., Cunha, R., Cabecinhas, D., Silvestre, C.: Robust global trajectory tracking for a class of underactuated vehicles. Automatica **58**, 90 – 98 (2015). DOI https://doi.org/10.1016/j.automatica.2015.05.011. URL `http://www.sciencedirect.com/science/article/pii/S0005109815002101`
3. Dierks, T., Jagannathan, S.: Output feedback control of a quadrotor uav using neural networks. IEEE Transactions on Neural Networks **21**(1), 50–66 (2010). DOI 10.1109/TNN.2009.2034145
4. Gao, S., Franco, C.D., Carter, D., Quinn, D., Bezzo, N.: Exploiting ground and ceiling effects on autonomous uav motion planning. In: 2019 International Conference on Unmanned Aircraft Systems (ICUAS), pp. 768–777 (2019). DOI 10.1109/ICUAS.2019.8798091
5. Hsiao, Y.H., Chirarattananon, P.: Ceiling effects for hybrid aerial–surface locomotion of small rotorcraft. IEEE/ASME Transactions on Mechatronics **24**(5), 2316–2327 (2019). DOI 10.1109/TMECH.2019.2929589

6. Khalil, H.: Nonlinear systems; 3rd ed. USA: Prentice-Hall, Upper Saddle River, NJ (2002)
7. Kocer, B.B., Tjahjowidodo, T., Seet, G.G.L.: Model predictive uav-tool interaction control enhanced by external forces. Mechatronics **58**, 47–57 (2019). DOI https://doi.org/10.1016/j.mechatronics.2019.01.004. URL `https://www.sciencedirect.com/science/article/pii/S0957415819300042`
8. Mahony, R., Kumar, V., Corke, P.: Multirotor aerial vehicles: Modeling, estimation, and control of quadrotor. IEEE Robotics Automation Magazine **19**(3), 20–32 (2012). DOI 10.1109/MRA.2012.2206474
9. Nekoo, S.R., Acosta, J.A., Ollero, A.: Collision avoidance of sdre controller using artificial potential field method: Application to aerial robotics*. In: 2020 International Conference on Unmanned Aircraft Systems (ICUAS), pp. 551–556 (2020). DOI 10.1109/ICUAS48674.2020.9213984
10. Nishio, T., Zhao, M., Shi, F., Anzai, T., Kawaharazuka, K., Okada, K., Inaba, M.: Stable control in climbing and descending flight under upper walls using ceiling effect model based on aerodynamics. In: 2020 IEEE International Conference on Robotics and Automation (ICRA), pp. 172–178 (2020). DOI 10.1109/ICRA40945.2020.9197137
11. Oliva-Palomo, F., Muñoz-Vázquez, A.J., Sánchez-Orta, A., Parra-Vega, V., Izaguirre-Espinosa, C., Castillo, P.: A fractional nonlinear pi-structure control for robust attitude tracking of quadrotors. IEEE Transactions on Aerospace and Electronic Systems **55**(6), 2911–2920 (2019). DOI 10.1109/TAES.2019.2893817
12. Sanchez-Cuevas, P.J., Heredia, G., Ollero, A.: Multirotor uas for bridge inspection by contact using the ceiling effect. In: 2017 International Conference on Unmanned Aircraft Systems (ICUAS), pp. 767–774 (2017). DOI 10.1109/ICUAS.2017.7991412
13. Silva, A.L., Santos, D.A.: Fast nonsingular terminal sliding mode flight control for multirotor aerial vehicles. IEEE Transactions on Aerospace and Electronic Systems **56**(6), 4288–4299 (2020). DOI 10.1109/TAES.2020.2988836
14. Song, J., Chang, D.E., Eun, Y.: Passivity-based adaptive control of quadrotors with mass and moment of inertia uncertainties. In: 2019 IEEE 58th Conference on Decision and Control (CDC), pp. 90–95 (2019)
15. Wang, H., Ye, X., Tian, Y., Zheng, G., Christov, N.: Model-free–based terminal smc of quadrotor attitude and position. IEEE Transactions on Aerospace and Electronic Systems **52**(5), 2519–2528 (2016)
16. Wang, X., Du, S., Liu, Y.: Research on ceiling effect of quadrotor. In: 2017 IEEE 7th Annual International Conference on CYBER Technology in Automation, Control, and Intelligent Systems (CYBER), pp. 846–851 (2017). DOI 10.1109/CYBER.2017.8446371
17. Xie, W., Yu, G., Cabecinhas, D., Cunha, R., Silvestre, C.: Global saturated tracking control of a quadcopter with experimental validation. IEEE Control Systems Letters **5**(1), 169–174 (2021). DOI 10.1109/LCSYS.2020.3000561
18. Zuo, Z., Ru, P.: Augmented $\mathcal{L}_1$ adaptive tracking control of quad-rotor unmanned aircrafts. IEEE Transactions on Aerospace and Electronic Systems **50**(4), 3090–3101 (2014)